Int. J. Electrochem. Sci., 13 **(2018)** 10440 – 10453, doi: 10.20964/2018.11.17

International Journal of
ELECTROCHEMICAL
SCIENCE
www.electrochemsci.org

Graphene Oxide Modified $LiNi_{1/3}Co_{1/3}Mn_{1/3}O_2$ as Cathode Material for Lithium Ion Batteries and Its Electrochemical Performances

Yuxin Ma[1,2], *Ping Cui*[2], *Bing Gan*[2], *Youliang Ma*[1], *Ying Liang*[1,2,*]

[1] School of Automobile and Traffic Engineering, Wuhan University of Science and Technology, Wuhan 430081, China
[2] School of Chemical Engineering and Food Science, Hubei University of Arts and Science, Xiangyang 441053, China
[*]E-mail: xfliangy@163.com

Received: 7 July 2018 / *Accepted:* 30 August 2018 / *Published:* 1 October 2018

$LiNi_{1/3}Co_{1/3}Mn_{1/3}O_2$(NCM) was coated with graphene oxide(GO) by a simple chemical approach. The prepared materials were characterised using various techniques such as X-ray diffraction (XRD), thermogravimetric analysis, scanning electron microscopy, energy dispersive spectroscopy, transmission electron microscopy and X-ray photoelectron spectroscopy. XRD revealed that the crystal structure and crystallinity do not change after surface modification with GO. The 2.5 wt% GO-coated NCM exhibits stable cycling stability with a capacity retention of 84.2% at 1 C after 100 cycles, which is higher than the corresponding value of 74.3% for the pristine sample. The rate performance results show that the GO coating increases the discharge capacity from 87.1 to 100.9 mAh g^{-1} at a high rate of 5 C. Therefore, GO-coated NCM is a highly promising cathode material for lithium-ion batteries because it provides good cycling stability and high rate performance.

Keywords: Lithium-ion battery; $LiNi_{1/3}Co_{1/3}Mn_{1/3}O_2$; GO; Electrochemical properties

1. INTRODUCTION

Advanced energy storage devices, such as lithium-ion batteries [1], supercapacitors [2], sodium-sulphur batteries [3] and solar cells [4], have been widely researched to address the global energy crisis and climate change problems. Among various forms of energy storage equipment, lithium-ion batteries have been regarded suitable power sources for battery electric vehicles, hybrid electric vehicles (HEVs) and parallel HEVs because of their high energy density, good cycling performance and long cycle life [5–7]. Lithium-ion batteries consist of cathodes, anodes and

electrolytes. However, the bottleneck problem that hinders the development of lithium-ion batteries is the limiting factor in high-performance cathode materials. $LiCoO_2$ [8] has been used as a cathode material in commercial LIBs because of its high charge/discharge voltage, good cycling ability and easy preparation; however, its low thermal stability, high cost and toxicity restrict its further development. $LiNiO_2$ [9] has been considered for use in second-generation commercial LIBs because of its high power and energy density, low cost and high discharge capacity; however, the chemical instability of Ni^{3+} ions makes it difficult to synthesise. $LiMn_2O_4$ [10, 11] has the advantages of low cost, high thermal stability and high voltage, but its reversible capacity fades rapidly at high current rates. Compared with other cathode materials, such as $LiCoO_2$, $LiNiO_2$ and $LiMn_2O_4$, layered $LiNi_xCo_yMn_{1-x-y}O_2$ has higher theoretical capacity, lower cost, higher safety and higher working voltage and environmentally friendly; it is also acknowledged as a promising candidate material for commercial LIBs. Recently, a series of $LiNi_xCo_yMn_{1-x-y}O_2$ was investigated including $LiNi_{1/3}Co_{1/3}Mn_{1/3}O_2$ [12], $LiNi_{0.5}Co_{0.2}Mn_{0.3}O_2$ [13], $LiNi_{0.6}Co_{0.2}Mn_{0.2}O_2$ [14] and $LiNi_{0.8}Co_{0.1}Mn_{0.1}O_2$ [15], in which the Ni content imparts a high charge/discharge capacity because of its redox reactions. However, the addition of Ni will cause cation mixing because the ionic radius of Li^+(0.76 Å) is similar to that of Ni^{2+}(0.69 Å), thus resulting in poor electrochemical performance. Among the $LiNi_xCo_yMn_{1-x-y}O_2$ mixed oxide series, NCM (111) has attracted great attention from academic and industrial engineers because of its high specific capacity, superior structural stability and environmental benignancy.

However, several drawbacks limit its further application. The first is the degradation of its reversible capacity during prolonged cycling because of an unstable surface layer between the electrode and electrolyte. The second is its poor rate capability, which can be attributed to poor electronic conductivity and side reactions with the cathode material. To overcome the shortcomings mentioned above, surface modification has proven to be an effective technique for improving the electrochemical performance of NCM. Thus, the most common coating materials including Al_2O_3 [16], MgO [17], TiO_2 [18], Nb_2O_5 [19], V_2O_5 [20], SrF_2 [21], $AlPO_4$ [22], Li_2ZrO_3 [23], Li_3VO_4 [24] and Li_2MnO_3 [25] have contributed to improvements in thermal stability and rate capacity. A suitable coating layer can act as a protective shell to prevent interfacial side reactions. However, most metal oxides have polarised the electrode and decreased the reversible capacity because of their inactivity with respect to lithium insertion/extraction. Therefore, it is essential to develop better conductive material to improve the electrochemical performance of NCM. Carbon is highly abundant and is associated with mature technologies. Therefore, its use in lithium-ion batteries should be pursued. Graphene oxide (GO), with its superior electronic conductivity, large specific surface area, stable chemical properties and mechanical strength, is considered an excellent conductive additive to nanostructure materials for lithium-ion batteries [26, 27]. In this work, we have explored the possibility of coating NCM particles with a layer of GO coating layer. GO was synthesised by a modified Hummers method, and a simple chemical approach was used to wrap it around NCM particles to improve their electrochemical performance. The influence of the GO coating on the cathode structure, morphology and electrochemical performance is discussed in detail. The satisfactory performance of GO-coated NCM (GO/NCM) renders it a promising cathode material that exhibits higher reversible capability, longer cycling stability and better rate capability than NCM.

2. EXPERIMENTAL

2.1. Synthesis of NCM

NCM was synthesised by a sol-gel citric acid assisted method. In a typical experiment, lithium acetate, nickel acetate, cobalt acetate and manganese, with a stoichiometric ratio of Li:(Ni+Co+Mn)=1.05:1, were selected as the starting materials and dissolved in ethyl alcohol. Excess 5% Li^+ was added to offset its loss, which occurs at high temperature. Citric acid solution was added dropwise to the above solution with vigorous stirring. The molar ratio of metal ions to citric acid was 1:1.2. The mixture was evaporated at 80°C with continuous stirring until a gel was formed, which was subsequently frozen at -80°C in a cryogenic refrigerator for 12 h, followed by freeze-drying for 24 h to acquire the precursor. The precursor was then heated at 450°C in air for 5 h with subsequent calcinations at 900°C for 12 h to obtain NCM.

2.2. Preparation of GO/NCM

GO/NCM was prepared by a simple chemical approach. First, GO was produced using a modified Hummers method [28, 29].Potassium persulphate (0.5 g), phosphorous pentoxide (0.5 g) and concentrated sulphuric acid (20 ml) were added into a 100 ml flask kept at 80°C; 1 g graphite powder was then placed in the flask, and the resultant dark blue mixture was kept at 80°C for 6 h. The pre-oxidised product was diluted with deionised water, washed and then filtered using a circulating water type vacuum pump until the syringe water pH=7. The pre-oxidised product was dried at 80°C for 8 h. Thereafter, 1 g of pre-oxidised product and 0.5 g $NaNO_3$ were dissolved in 23 ml of 98% H_2SO_4 at 0°C and 3 g $KMnO_4$ was slowly added, keeping the temperature of the suspension below 5°C with an ice bath. The mixture was heated to 35°C and stirred for 3 h before adding distilled water (80 ml). The mixture was then heated to 98°C and further stirred for 30 min before adding 3% H_2O_2 solution (10 ml) to remove the remaining $KMnO_4$, after which the colour of the mixture changed to bright yellow. The mixture was filtered and washed with 10% HCl solution to remove the residual metal ions and acids and was maintained at pH=7. The material was frozen at -80°C in a cryogenic refrigerator for 12 h, followed by freeze-drying for 24 h. Thus, the GO sample was obtained.

GO (25 mg) was dispersed in 30 ml ethanol with ultrasonication for 3 h to ensure that it was completely dissolved. Thereafter, 1 g of NCM powder was immersed in the mixture with vigorous stirring, and the mixture was heated at 60°C until the alcohol completely evaporated. Finally, the obtained material was placed in a freeze dryer at -50°C for 10 h.

2.3. General characterization

The crystal structure was analysed by X-ray diffraction (XRD) (D8 advance, Bruker) with Cu-Kα radiation (40 kV, 40 mA) in the 2θ range 10°–80° at a scan rate of 10°/min. The particle site, surface morphologies and elemental composition of the samples were performed by scanning electron microscopy (SEM) (S-4800, Hitachi) equipped with energy dispersive spectroscopy (EDS).

Thermogravimetric analysis (TGA) (AQ20, TA) was performed from room temperature to 900°C at a heating rate of 10°/min in air. Transmission electron microscopy (TEM) (Talos F200S, FEI) was employed to estimate the thickness of the coating on the surface of the cathode powders. X-ray photoelectron spectroscopy (XPS) (Thermo Scientific ESCALAB 250Xi) was used to evaluate the ion valence states in the metal oxide.

2.4. Electrochemical measurements

The electrochemical properties of pristine and GO/NCM were measured using a CR2032 coin cell. The electrodes were prepared by mixing the active material with acetylene black and polyvinylidene fluoride (80:10:10) in N-methyl-2-pyrrolidone to obtain a slurry, which was coated on cleaned and polished aluminum foil and dried at 80°C for 10 h in a vacuum oven. The cells were assembled in an argon-filled glove box, in which water and oxygen levels were maintained below 1ppm. $LiPF_6$ (1 M) dissolved in an EC: DMC (1:1 vol.%) electrolyte. The cells consist of a prepared cathode, with lithium metal as an anode and a polypropylene microporous film (Celgard 2400) as the separator. The weight of active material in the electrode was 3 mg/cm^2. A galvanostatic charge–discharge test was performed at rates of 0.2, 0.5, 1, 2 and 5 C in the voltage range 2.5–4.3 V at room temperature. Electrochemical impedance spectroscopy (EIS) was also conducted on an Autolab PGSTAT302N in the frequency range 100–0.01 Hz with a potential perturbation of 5 mV.

3. RESULTS AND DISCUSSION

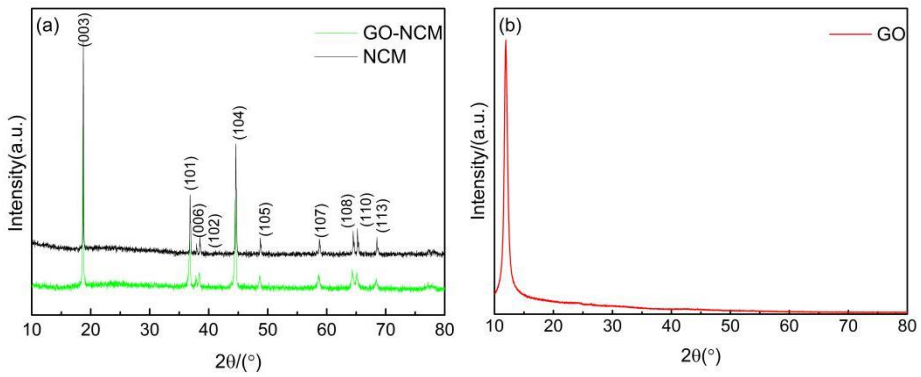

Figure 1.XRD patterns of NCM and GO/NCM (a) and GO(b).

The chemical compositions and crystal structures of NCM and GO/NCM were determined by XRD. As shown in Fig.1(a), all the diffraction peaks are sharp and well-defined, thus indicating that the synthesised materials are well-crystallised. All the materials can be indexed as layered oxide structures based on a hexagonal α-$NaFeO_2$ structure with an $R\bar{3}m$ space group, with no impurity phases detected [30]. The splitting of the (006)/(102) and (108)/(110) peaks at 38° and 65° is clearly

identified, thus indicating that the materials have highly ordered layered structures [31]. The XRD pattern of GO shown in Fig.1(b) has a sharp peak at 11°, which can be attributed to the complete oxidation of graphite to graphite oxide [32]. However, no diffraction peaks of GO can be observed in the XRD patterns of GO/NCM. This is probably because the strong diffraction peaks from the highly crystalline NCM and the coated GO (2.5 wt%) are below the detection limit of XRD [33, 34]. The calculated lattice parameters (a and c) for NCM (a=2.857 Å and c=14.205 Å) and GO/NCM (a=2.860 Å and c=14.230 Å) are in accordance with those reported in the literature[35, 36].The intensity ratio I(003)/I(104) is a sensitive parameter with respect to the degree of cation mixing of the samples. In a previous study, in which I(003)/I(104)>1.2, it was confirmed that the material possessed a good layer structure with low cation mixing [37]. In the present study, the I(003)/I(104) values for the NCM and GO/NCM powders were calculated as 1.28 and 1.32, respectively. All the results indicate that the crystal structure and crystallinity do not change after surface modification with GO.

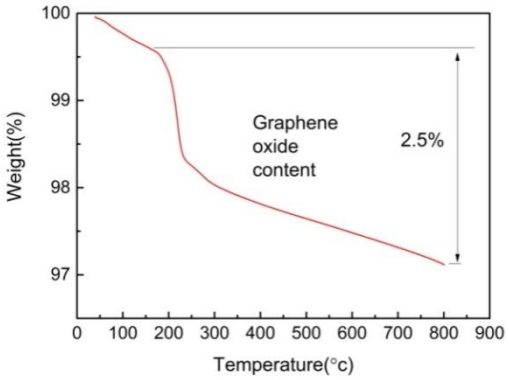

Figure 2. TG curves of GO/NCM composite.

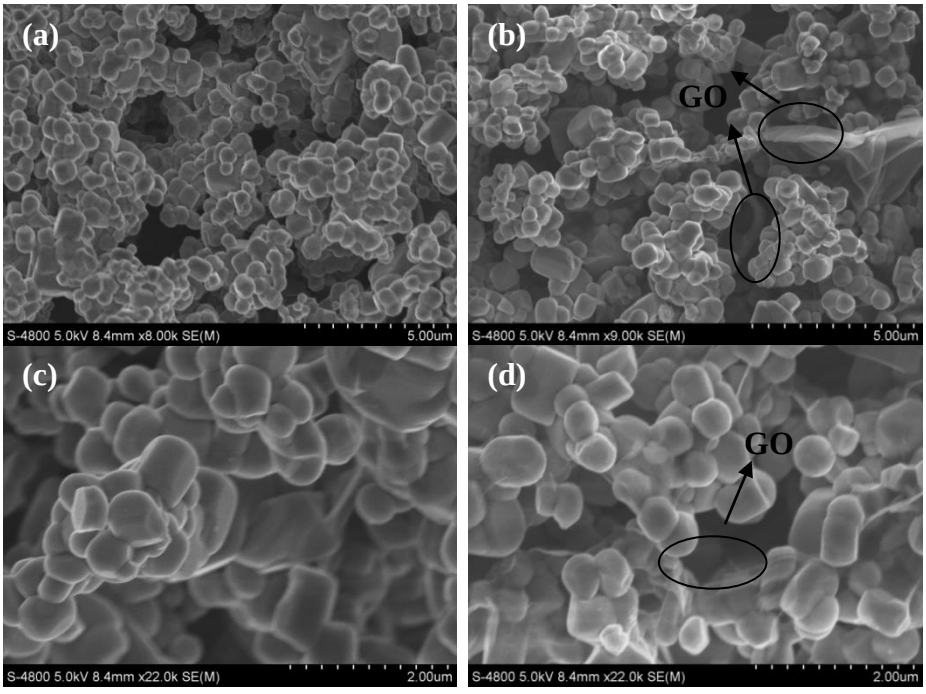

Figure 3. SEM images of bare (a and c) and GO/NCM cathodes (b and d).

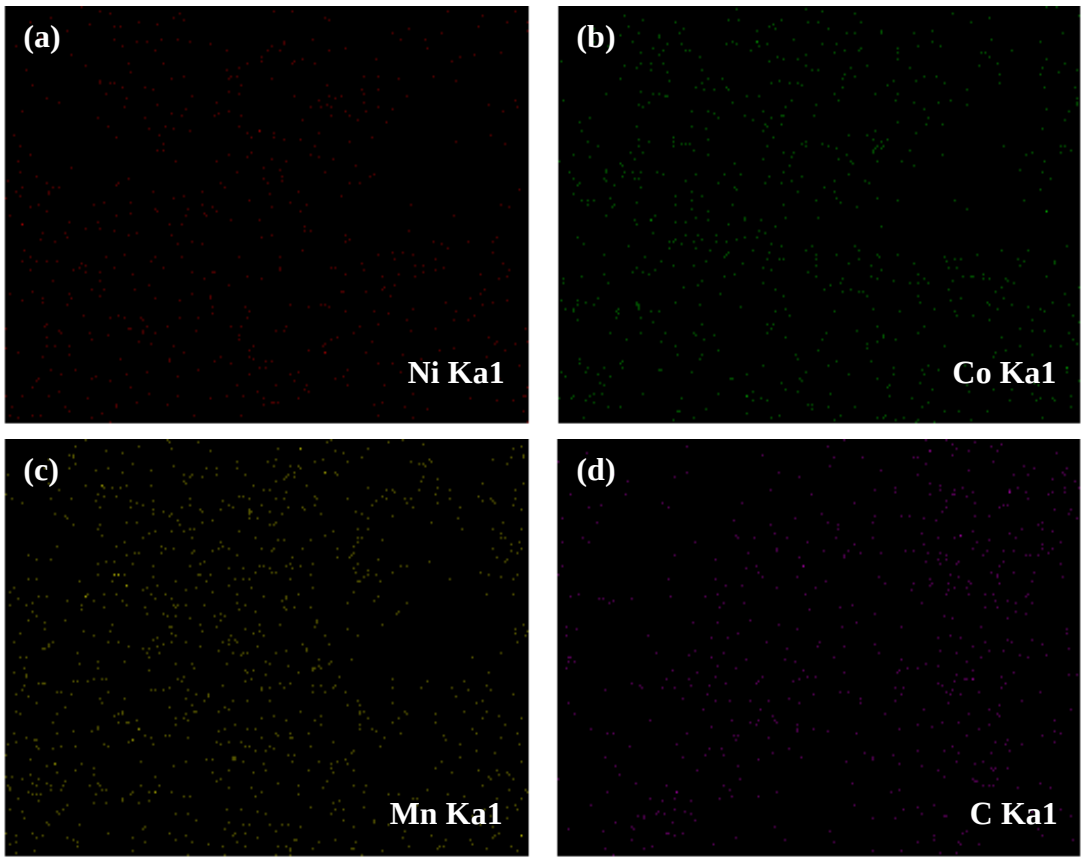

Figure 4. EDS maps of GO-NCM.

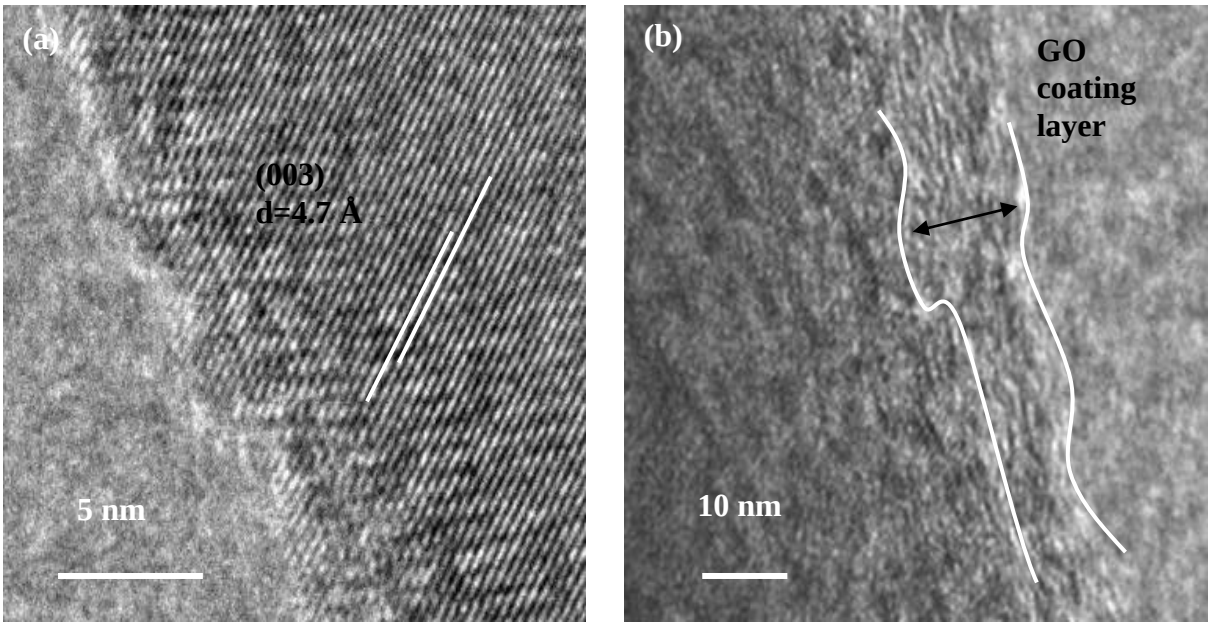

Figure 5. HRTEM micrographs of NCM (a) and GO/NCM (b).

TGA was used to quantify the amount of GO present in the GO/NCM composites. Fig.2 shows the thermogravimetric (TG) curves of the GO/NCM when it was healed from 25°C to 900°C at a rate of 5°/min. According to the TG curve, the weight loss of GO (0.5%) below 200°C resulted from the

removal of absorbed water molecules from its surface. The weight loss from 200°C to 350°C was due to the decomposition of oxygen-containing functional groups in the GO sheets, and the weight loss above 350°C was due to the combustion of carbon skeleton [38]. The TG results confirm that the content of GO in the NCM cathode material is 2.5%.

The apparent morphologies of NCM and GO/NCM were examined by SEM, as shown in Fig.3. Both samples consisted of homogeneous primary particles with average particle sizes of 200–500 nm. The images of the GO/NCM composite show NCM particles embedded in the GO sheets. The uniform GO/NCM structures can be ascribed to the simple chemical mixing method. Furthermore, continuous stirring and ultrasonication were effective in distributing the materials throughout the GO sheets. Thus, the GO network provides conductive connections between the NCM particles. EDS was also used to confirm the distribution of the GO coating layer on the surface of NCM. As illustrated in Fig.4, elemental C originating from GO was uniformly distributed throughout the cathode material, thus indicating that the cathode material is successfully and evenly coated with GO via this simple chemical approach.

To further confirm the formation of the coated structure, high-resolution TEM (HRTEM) was performed to evaluate the interplanar spacing and observe the microstructures of the coated materials. The bare sample presents perfect crystallinity in Fig.5a, with clear lattice fringes extending to the particle boundary. The interplanar spacing of the parallel lattice is approximately 4.7 Å, which corresponds to the spacing of the (003) plane of the hexagonal layered structure [39]. Fig.5b shows the GO coating layer on the surface of NCM with a thickness approximately 10–12 nm, and an obvious gap was found between the GO and the cathode material. This finding indicated tight adhesion between GO and NCM.

The modification of NCM with GO, can lead to the transition metals (Ni, Co, Mn) changing their oxidation states and result in low discharge capacity and poor cycling performance. Thus, XPS measurements were performed to detect the valence state of the transition metals in the GO/NCM materials. The results are shown in Fig.6. The XPS wide spectra show that GO/NCM has Li1s, Ni2p, Co2p, Mn2p, C1sand O1s peaks. The binding energies of $Ni2p_{3/2}$, $Co2p_{3/2}$ and $Mn2p_{3/2}$ for GO/NCM are 855.3, 780.1 and 624.6 eV, respectively, thus suggesting that Ni, Co, and Mn in our materials are respectively divalent, trivalent and tetravalent, which is consistent with reported values [40]. Two major peaks at about emerge in the Ni2p spectrum (Fig.6b); these peaks are assigned to the $Ni2p_{3/2}$ and $Ni2p_{1/2}$ peaks. The presence of a satellite peak can be attributed to the multiple splitting of nickel oxide energy levels [41]. The electron binding energies of $Co2p_{3/2}$ and $Co2p_{1/2}$ were recorded at 780.1 and 795.5 eV, thus implying that the existence of Co^{3+}. The $Mn2p_{3/2}$ energy at 646.2 eV confirms Mn^{4+} oxidation states in the samples [42]. The C1s spectra of the materials are deconvoluted into three main peaks. The peaks with binding energies of 288.5, 285.2 and 284.5 eV are ascribed to carboxyl groups (–O–C=O), hydroxyl groups (C–OH) and carbon networks (C–C/C=C), respectively [43]. The results indicate that GO in the 2.5 wt% GO/NCM has no impact on the valence state of the transition metals.

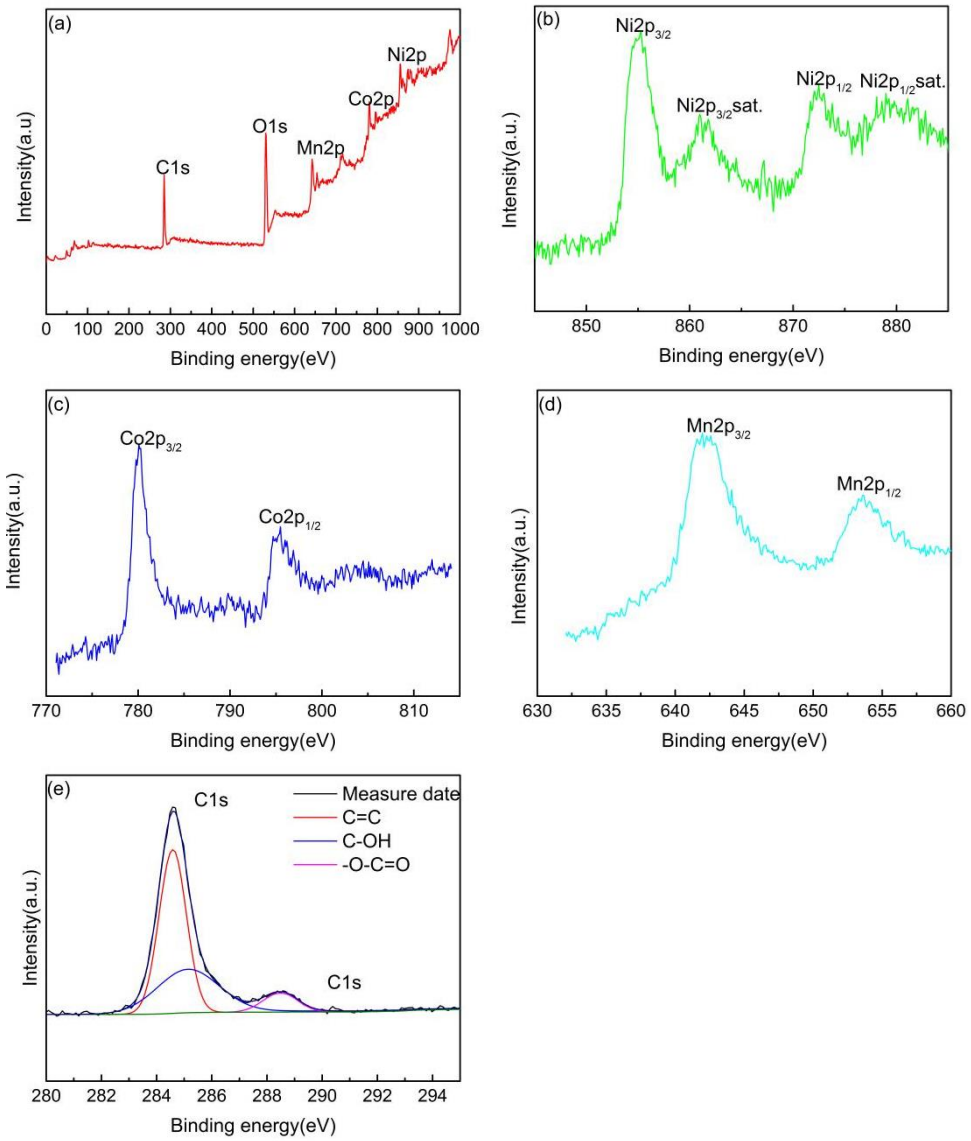

Figure 6. XPS spectra of GO/NCM for all elements(a), Ni2p(b), Co2p(c), Mn2p(d) and C1s(e).

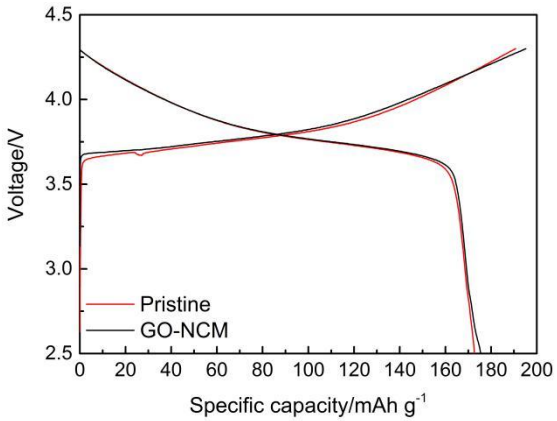

Figure 7. Initial charge/discharge curves of the bare and GO/NCM samples.

Fig.7 shows the initial charge-discharge curves of the bare and 2.5 wt% GO/NCM samples at 0.1 C in the voltage range 2.5–4.3 V. All charge-discharge curves had a potential plateau at 3.6 V, consistent with a typical-layer-structured NCM. At room temperature, the initial charge-discharge capacities for GO/NCM and NCM are 195.8/177.2 and 190.7/172.6 mAh g^{-1}, respectively. It is clear that the GO plays an important role in improving the capacity of the cathode materials. The increased discharge capacity of GO/NCM is mainly attributed to two factors. Firstly, coating GO, which has a large surface area, on the surface of NCM increases the contact area between the cathode material and electrolyte, further improving the performance of the active material. Secondly, lithium storage on the GO sheets could also reduce the electrochemical polarisation during charge/discharge.

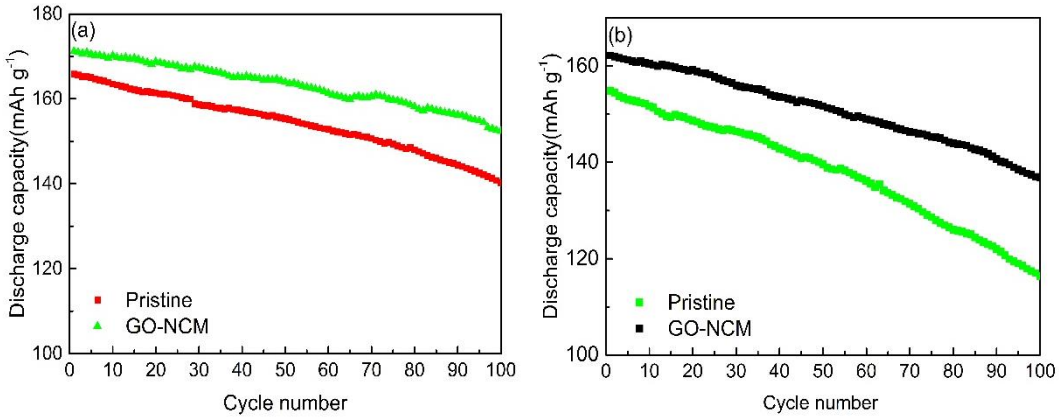

Figure 8. Cycling performances of NCM and GO-NCM samples at 0.2C (a) and 1C (b) after 100 cycles.

Fig.8(a) shows the cycling performances of the NCM and 2.5 wt% GO/NCM electrodes at a constant current of 0.2 C between 2.5 and 4.3 V at room temperature. The NCM delivers initial capacities of 165.8 mAh g^{-1} after 100 cycles, and it retains a capacity of 140.3 mAh g^{-1} with a capacity retention of 84.6%. On the contrary, the 2.5 wt% GO/NCM materials deliver initial discharge capacities of 152.4 mAh g^{-1} after 100 cycles, corresponding to a capacity retention of 89%. This suggests that the GO coating layer on the NCM surface enhanced its cycling stability and capacity retention.

To observe the effect of the coating on the high-rate material cycling performance, the cells were measured at a current density of 1 C between 2.5 and 4.3 V. The corresponding results are shown in Fig.8 (b). The discharge capacity of NCM decreased from 154.9 to 115.1 mAh g^{-1} after 100 cycles, with a capacity retention of only 74.3%. On the contrary, 2.5 wt% GO/NCM delivered a discharge capacity of 162.5 mAh g^{-1} in the first cycle and 136.8 $mAhg^{-1}$ after 100 cycles, with a corresponding capacity retention of 84.2%. Comparing the cycle performances at 0.2 C, GO/NCM performed slightly better than the bare NCM; however, at 1 C, GO/NCM exhibited remarkable improvement compared with bare NCM. The better cycling performance of GO/NCM can be ascribed to the protection by the GO coating layer, which reduced the corrosion of the cathode material by the electrolyte and suppressed side reactions between the active material and electrolyte during the prolonged cycling [44].

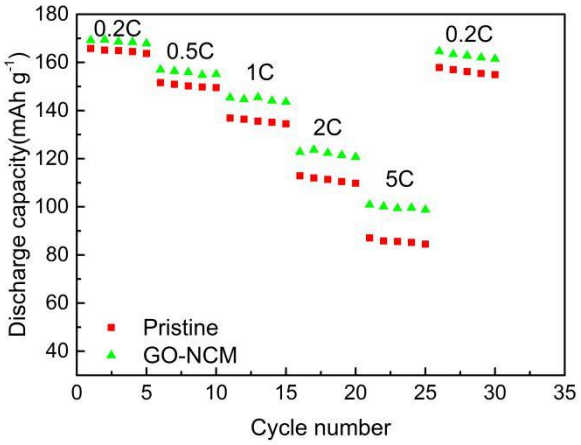

Figure 9. Rate performance of the NCM and GO/NCM samples.

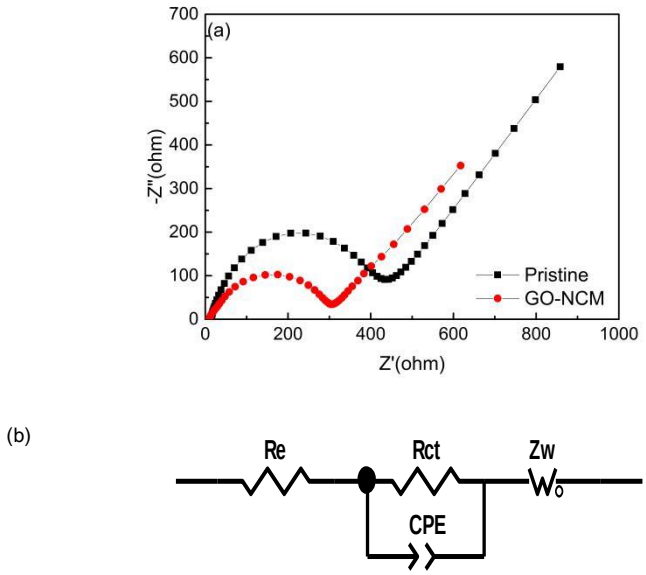

Figure 10. (a) Nyquist plots of NCM and GO/NCM electrodes after 100cycles. (b) Equivalent circuit model.

The rate performances of the bare and GO/NCM cathodes are shown in Fig.9. The cells were charged and discharged between 2.5 and 4.3 V vs. Li/Li^+ at current rates of 0.2, 0.5, 1, 2 and 5 C. The rate was increased from 0.2 to 5 C stepwise and finally returned to 0.2 C every five cycles at each current rate. All the cathodes exhibited gradual decreases in discharge capacity as the current density increased. The 2.5 wt% GO/NCM sample presented a distinctly improved discharge capacity compared with NCM (100.9 vs. 87.1 mAh g^{-1}) at a current density of 5 C. However, when the current density was decreased to 0.2 C again, the capacity of GO/NCM almost recovered its initial value, thus

implying that a high current density and rapid lithiation/delithiation do no effect the crystal structure. By contrast, the NCM did not recover its initial capacity because of an irreversible capacity loss resulting from an increase in its inner resistance. The GO introduced into the NCM material improved the reaction kinetics by increasing the electrical conductivity via the GO 2D network.

EIS measurements were performed to further investigate the possible reasons why the GO-coated NCM improves the electrochemical performance and reaction kinetics, particularly at high current rates. Fig.10 displays the impedance spectrum obtained with a coin cell after the 100th charge–discharge cycle. All these curves consist of a single semicircle in the high-to medium-frequency region and a quasi-linear line in the low-frequency region [45]. In general, the semicircle in the high-to medium-frequency region is related to the charge transfer resistance (R_{ct}), and the quasi-linear line in the low-frequency region is attributed to the Warburg impedance (Z_w), which is ascribed to lithium-ion diffusion in the solid phase of the electrode [46,47]. The equivalent electrical circuit is shown in Fig.10(b), where R_e represents the solution resistance, CPE stands for the double layer capacitance and R_{ct} represents the charge transfer resistance. The values of R_e and R_{ct} were obtained by fitting with Zview software.

After the 100th cycle, R_{ct} for the pristine samples was 362 Ω. However, for the 2.5 wt% GO/NCM, R_{ct} was only 247 Ω. This directly demonstrates that a minimum amount GO-coated on the electrode improved the diffusion of Li ions, increased the electrical conductivity and suppressed the increase in resistance. Furthermore, the GO-coating layer can inhibit side reactions between the electrode and electrolyte during the high-rate charge-discharge process, thus slowing down the increase in the charge transfer resistance (R_{ct}). The large surface area and better electrical conductivity of GO lead to a reduction in the charge transfer resistance of the coated cathode material, thus enhancing the electrode kinetics and consequently resulted in a superior electrochemical performance.

To further study the electrical conductivity for the bare and GO/NCM, the diffusion coefficient of lithium ions can be evaluated according to the following equation [48, 49]:

$$D_{\mathrm{Li}} = \frac{R^2T^2}{2A^2n^4F^4C^2\sigma^2} \quad (1)$$

where R is the gas constant (8.314 $\mathrm{Jmol^{-1}K^{-1}}$), T is the absolute temperature (298.15 K), A is the surface area of the electrode, n is the number of electrons per molecule during Li ion insertion, F is the Faraday constant (96486 $\mathrm{Cmol^{-1}}$), C is the lithium-ion concentration and σ is the Warburg factor, which can be obtained using the following equation:

$$Z' = R_e + R_{ct} + \sigma\omega^{-1/2} \quad (2)$$

R_e is the solution resistance; R_{ct} is the charge transfer resistance and ω is the angular frequency. Fig.11 shows the linear relationship between Z' and $\omega^{-1/2}$ (square root of frequency) in the low-frequency region. The lithium-ion diffusion coefficients of NCM and GO/NCM were calculated are 5.29×10^{-13} and 7.92×10^{-13} $\mathrm{cm^2/s}$.

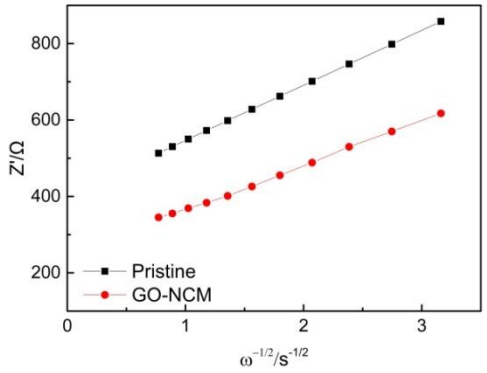

Figure 11. The relationship between Z' and $\omega^{-1/2}$ ($s^{-1/2}$) for NCM and GO/NCM.

The improved D_{Li} for the GO/NCM particles due to the large surface area of GO sheets allows the fabrication of a binder free cathode, which also enhances the electrical conductivity and facilitates electrolyte through the cathode. Thus, the GO coating layer increases the lithium-ion diffusion coefficient compared with the NCM samples.

4. CONCLUSIONS

In summary, NCM was coated with GO through a simple chemical approach. The 2.5 wt% GO/NCM retained its original crystal structure and even exhibited better electrochemical performance than the pristine material in terms of discharge capacity, high columbic efficiency, rate capacity, cycling performance and lithium-ion diffusion coefficient. These performance improvements are mainly ascribed to the GO coating layer, which has a large surface area and better electrical conductivity. Thus, GO not only prevented the side reaction between the active material and electrolyte but also stabilised the crystal structure at high current densities. GO-coated NCM is a promising cathode material candidate for potential applications in electric vehicles and HEVs.

ACKNOWLEDGEMENT
This work was financially supported by the National Science Foundation of China (Grant NO.51378183) and the Research Program of Hubei Provincial Department of Education (T201215), and the Petroleum and Chemical Industry Federation Program of China (Grant NO.20170902).

References

1. P. Poizot, S. Laruelle, S. Grugeon, L. Dupont and J.M. Tarascon, *Nature*, 407 (2000) 496.
2. R.F. Service, *Science*, 313 (2006) 902.
3. C.W. Park, H.S. Ryu, K.W. Kim, J.H. Ahn, J.Y. Lee and H.J. Ahn, *J. Power Sources*, 165 (2007) 450.

4. J. Nelson, *Science*, 293 (2001) 1059.
5. J.M. Tarascon, M. Armand, *Nature*, 414 (2001) 359.
6. N. Loeffler, D. Bresser, S. Passerini and M. Copley, *Platin.Met.Rev.,* 59 (2015) 34.
7. A. Scott, *Chem. Eng. News,* 93 (2015) 18.
8. Y. Takahashi, S. Tode, A. Kinoshita, H. Fujimoto, I. Nakane and S. Fujitani, *J. Electrochem. Soc.,* 155 (2008) A537.
9. A.W. Moses, H.G.G. Flores, J.G. Kim and M.A. Langell, *Appl.Surf. Sci.,* 253 (2007) 4782.
10. S. Sengupta, R.R. Roy, A. McLean and S. Dasgupta, *Can. Metall. Q.,* 45 (2006) 341.
11. H.M. Wu, J.P. Tu, X.T. Chen, Y. Li, X.B. Zhao and G.S. Cao, *J. Electroanal. Chem.,* 586 (2006) 180.
12. R. Santhanam, B. Rambabu, *J. Power Sources*, 195 (2010) 4313.
13. D. Aurbach, O. Srur-Lavi, C. Ghanty, M. Dixit, O. Haik, M. Talianker, et al. *J. Electrochem. Soc.,* 162 (2015) A1014.
14. H. Kaneda, Y. Koshika, T. Nakamura, H. Nagata, R. Ushio and K. Mori, *Int. J. Electrochem. Sci.,* 12 (2017) 4640.
15. K. Meng, Z. Wang, H. Guo, X. Li and D. Wang, *Electrochim. Acta,* 211 (2016) 822.
16. K. Araki, N. Taguchi, H. Sakaebe, K. Tatsumi and Z. Ogumi, *J. Power Sources*, 269 (2014) 236.
17. J.B. Li, Y.L. Xu, L.L. Xiong and J.P. Wang, *Acta Phys.-Chim. Sin.,* 27 (2011) 2593.
18. J. Li, M. Fan, X. He, R. Zhao, C. Jiange and C. Wan, *Ionics*, 12 (2006) 215.
19. S. Uchida, N. Zettsu, K. Hirata, K. Kami and K. Teshima, *RSC Adv.,* 6 (2016) 67514.
20. X. Liu, P. He, H. Li, M. Ishida and H. Zhou, *J. Alloys Compd.,* 552 (2013) 76.
21. J. Li, L. Wang, Q. Zhang and X. He, *J. Power Sources*, 190 (2009) 149.
22. J.H. Wang, Y. Wang, Y.Z. Guo, Z.Y. Ren and C.W. Liu, *J. Mater. Chem.,* A1 (2013) 4879.
23. W. Wang, Z. Yin, J. Wang, Z. Wang, X. Li and H. Guo, *J. Alloys Compd.,* 651 (2015) 737.
24. W. Wang, Z. Yin, Z. Wang, X. Li, H. Guo and D. Wang, *J. Alloys Compd.,* 646 (2015) 454.
25. J. Li, Y. Xu, X. Li and Z. Zhang, *Appl. Surf. Sci.,* 285 (2013) 235.
26. S. Stankovich, D.A. Dikin, R.D. Piner, K.A. Kohlhaas, A. Kleinhammes, Y. Jia, et al. *Carbon*, 45 (2007) 1558.
27. B. Song, M.O Lai, Z. Liu, H. Liu and L. Lu, *J. Mater. Chem.,* A1 (2013) 9954.
28. W.S. Hummers, R.E. Offeman, *J. Amer. Chem. Soc.,* 80 (1958) 1339.
29. N.I. Kovtyukhova, P.J. Ollivier, B.R. Martin, T.E. Mallouk, S.A. Chizhik, E.V. Buzaneva and A.D. Gorchinskiy, *Chem. Mater.,* 11 (1999) 771.
30. K.M. Shaju, G.V.S Rao, B.V.R Chowdari, *Electrochim. Acta,* 48 (2002) 145.
31. Q. Wang, N. Tian, K. Xu, L. Han, J. Zhang, W. Zhang, et al. *J. Alloys Compd.,* 686 (2016) 267.
32. Y. Ji, L. Qi, M. Cheng, L. Lai, Z. Li, Y. Peng, et al. *Mater. Sci. Eng. C,* 33 (2013)3811.
33. S.S Jan, S. Nurgul, X. Shi, H. Xia and H. Pang, *Electrochim. Acta,* 149 (2014) 86.
34. Z.M. Luo, Y.G. Sun, H.Y. Liu, *Chin. Chem. Lett.,* 26 (2015) 1403.
35. H. Zhu, J. Li, Z. Chen, Q. Li, T. Xie, L. Li, et al. *Synthetic Metals*, 187 (2014) 123.
36. J.Z. Kong, H.F. Zhai, C. Ren, M.Y. Gao, X. Zhang, H. Li, J.X. Li, Z. Tang and F. Zhou, *J. Alloys Compd.,* 577 (2013) 507.
37. N. Yabuuchi, T. Ohzuku, *J. Power Sources*, 119–121 (2003) 171.
38. P. Liu, K. Gong, P. Xiao, M. Xiao, *J. Mater Chem.,* 10 (2000) 933.
39. C. Lin, Y. Zhang, L. Chen, Y. Lei, J. Ou, Y. Guo, et al. *J. Power Sources*, 280 (2015) 263.
40. P. Manikandan, M.V. Ananth, T.P. Kumar, M. Raju, P. Periasamy and K. Manimaran, *J. Power Sources*, 196 (2011) 10148.
41. P. Manikandan, P. Periasamy, *Mater.Res. Bull.,* 50 (2014) 132.
42. Q. Jiang, K. Du, Y. He, *Electrochim. Acta,* 107 (2013) 133.
43. T.H.T. Vu, T.T.T Tran, N.T.L. Hong, L.T. Tran, P.H.T. Nguyen, M.D. Nguyen, et al. *Mater. Res. Bull.,* 73 (2016) 197.
44. G.L. Jia, C.M. Jiao, W.J. Xue, S.H. Zheng and J. Wang, *Solid State Ionics*, 292 (2016) 15.

45. C.J. Jafta, K.I. Ozoemena, M.K. Mathe and W.D. Roos, *Electrochim. Acta,* 85 (2012) 411.
46. S.Y. Tan, L. Wang, B. Liang, J.B. Xu, W. Ren, P.F. Hu, et al. *J. Power Sources*, 277 (2015) 139.
47. M. Wang, M. Luo, Y. Chen, Y. Su, L. Chen and R. Zhang, *J. Alloys Compd.,* 696 (2016) 907.
48. N. Takami, A. Satoh, M. Hara and T. Ohsaki, *Cheminform*, 26 (1995) .
49. A.J. Bard, L.R. Faulkner, *Electrochemical Methods, second ed.,* Wiley, (2001) New Jersey, American